Nanoscale Detection of Ionizing Radiation Damage to DNA by Atomic Force Microscopy

Changhong Ke, Yong Jiang, Piotr A. Mieczkowski, Garrett G. Muramoto, John P. Chute, and Piotr E. Marszalek*

*T*he detection and quantification of ionizing radiation damage to DNA at a single-molecule level by atomic force microscopy (AFM) is reported. The DNA damage-detection technique combining supercoiled plasmid relaxation assay with AFM imaging is a direct and quantitative approach to detect gamma-ray-induced single- and double-strand breaks in DNA, and its accuracy and reliability are validated through a comparison with traditional agarose gel electrophoresis. In addition, the dependence of radiation-induced single-strand breaks on plasmid size and concentration at a single-molecule level in a low-dose (1 Gy) and low-concentration range (0.01 ng μL^{-1}–10 ng μL^{-1}) is investigated using the AFM-based damage-detection assay. The results clearly show that the number of single-strand breaks per DNA molecule is linearly proportional to the plasmid size and inversely correlated to the DNA concentration. This assay can also efficiently detect DNA damage in highly dilute samples (0.01 ng μL^{-1}), which is beyond the capability of traditional techniques. AFM imaging can uniquely supplement traditional techniques for sensitive measurements of damage to DNA by ionizing radiation.*

Keywords:
- atomic force microscopy
- DNA
- gamma radiation
- single-molecule studies

1. Introduction

Exposure to ionizing radiation can produce severe consequences in humans and animals, such as acute hematologic, gastrointestinal, and neuronal toxicity and is associated with an increased long-term risk of carcinogenesis.[1–3] Random energy deposition by ionizing radiation damages many cellular components and may result in a variety of direct and indirect DNA lesions.[4,5] Ionizing radiation-induced DNA damage has been intensively investigated during the past few decades. It was found that DNA in human cells can be significantly damaged even at low doses of ionizing radiation < 1 Gy.[6] The majority of direct lesions are single- and double-strand breaks, the latter being the most deleterious. The majority of indirect lesions are caused by hydroxyl radicals (·OH), which are created upon water radiolysis and can cause single- and double-strand breaks (SSB and DSB), and base and sugar damage. One of the established methodologies to investigate the mechanisms of

[*] C. Ke, Y. Jiang, Dr. P. E. Marszalek
Center for Biologically Inspired Materials and
Material Systems and Department of Mechanical
Engineering and Materials Science, Duke University
Durham, NC 27708 (USA)
Fax: (+1) 919-660-8963
E-mail: pemar@duke.edu

Dr. P. A. Mieczkowski
Department of Molecular Genetics and Microbiology
Duke University Medical Center
Durham, NC 27708 (USA)

G. G. Muramoto, J. P. Chute
Division of Cellular Therapy
Department of Medicine
Duke University
Durham, NC 27708 (USA)

gamma (γ)- ray-induced damage to isolated DNA is the supercoiled plasmid relaxation assay.[5,7–13] Supercoiled plasmid DNA molecules, when exposed to γ-rays, are converted into their relaxed circular or linear forms, as a result of SSBs and DSBs, respectively. The numbers of induced SSBs and DSBs are dependent on several factors, including radiation dose and DNA buffer conditions, such as the presence or absence of free-radical scavengers.[14]

The traditional techniques to evaluate DNA damage that involve the use of the supercoiled plasmid relaxation assay employ the separation of the three DNA topoisomers by methods such as gel electrophoresis[15] or liquid chromatography,[16,17] followed by the quantification of each DNA form by spectrophotometry,[18] fluorometry,[19–22] or autoradiography.[23]

Atomic force microscopy (AFM) is an imaging technique[24] that is able to resolve single molecules and even individual large atoms. AFM has been successfully applied to image various forms of DNA[8,25–27] including supercoiled plasmids and it has easily resolved their topological variants.[7,9,11,28–32] Because of its very high imaging resolution and the ability to image under ambient conditions, including liquid form, AFM has established itself as an important technique in DNA research. However, the application of AFM in studies of DNA damage has, so far, been quite limited,[7,11,33,34,35] even though AFM has some unique advantages, such as the extremely small amounts of DNA material needed and an ability to directly visualize, count, and measure sizes of different topological forms of DNA at a single-molecule level, without any need for a spatial separation of these forms or labeling (staining) of damaged DNA, to facilitate its quantification.[35] Direct counting of the numbers of supercoiled, circular, and fragmented (linear) duplexes from AFM images allows accurate determination of the distributions of SSBs and DSBs in a straightforward way with no need to apply complex and approximate mathematical models.[11,35] Because of these features, AFM imaging seems to be ideal for quantifying radiation-induced SSBs and DSBs in supercoiled DNA, under a wide range of DNA concentrations and DNA sizes that may be less accessible by other methods (e.g., when extremely dilute samples, with DNA concentrations, $C < 0.01$ ng μL^{-1} are used, or when very large plasmids are employed). It has been demonstrated that AFM is capable of imaging DNA plasmids with sizes up to 100 kilobase pairs (kbp).[36] The wider use of AFM techniques in research focused on DNA damage is impeded by the lack of careful studies to verify this novel method against other traditional and well-established methods, such as separating DNA by agarose gel electrophoresis.[13,37,38] Cross-checking the results obtained by AFM with the results obtained by other well-established techniques is particularly important in light of earlier studies suggesting some discrepancies between the data obtained by AFM and by gel electrophoresis.[9] This apparent discrepancy is likely to have originated because the differences in fluorescence intensities produced by different topological fractions of DNA during gel electrophoresis measurements[19,39] were not accounted for and are likely to have skewed the fractions of various DNA forms detected on the gel.[9] In addi-

tion, while the effect of radiation dose on the number of produced SSBs and DSBs has been studied quite extensively using traditional methods,[6,40–43] the effects of the size and concentration of supercoiled DNA on the numbers of these lesions have so far been considered only superficially.[41] Therefore, the purpose of this paper is to validate single-molecule AFM imaging as a new means for sensitive and quantitative detection of SSBs and DSBs in irradiated DNA and to thoroughly examine the dependence of damage detection sensitivity on plasmid size and DNA concentration. We believe that this report will help to expand the use of AFM techniques in nanoscale DNA damage research.

2. Results and Discussion

2.1. Comparison of DNA Damage Detection by AFM Imaging and by Agarose Gel Electrophoresis

We investigated the accuracy of our AFM-based DNA damage-detection assay by comparing the distribution of various topological forms of irradiated DNA obtained by AFM imaging with the amounts of DNA measured in various bands, after separating the irradiated plasmids by agarose gel electrophoresis. Because plectonemic supercoiled DNA is underfluorescent compared to circular and linear forms,[19,39] which produce similar amounts of fluorescence, a correcting factor has to be determined and taken into account when measuring the relative amounts of DNA in different bands, based on band intensity, as determined by a charge-coupled device (CCD) camera. Such correction factors were found to be dependent on many experimental conditions, including plasmid type, dye concentration, and agarose and buffer type and concentration.[13] Therefore, the correction factor needs to be determined for each specific experimental system. To determine the correction factor for our model DNA, the pUC18 plasmid, we prepared two master solutions containing supercoiled pUC18 plasmid and its linearized version, both at 1 ng μL^{-1} in PBS buffer. Five 100-μL DNA samples containing the supercoiled pUC18 plasmids and linear pUC18 with known ratios were separated by gel electrophoresis. The results are shown in Figure 1, in which lanes 1 through 5 correspond to the following DNA mixtures:

1) 100 ng supercoiled pUC18, 0 ng linear pUC18
2) 75 ng supercoiled pUC18, 25 ng linear pUC18
3) 50 ng supercoiled pUC18, 50 ng linear pUC18
4) 25 ng supercoiled pUC18, 75 ng linear pUC18
5) 0 ng supercoiled pUC18, 100 ng linear pUC18

The quantity of DNA in each band was measured based on the band intensity, as plotted in Figure 2. It can be clearly seen that for both supercoiled plasmid pUC18 and linear pUC18, the intensity of the band is linearly correlated with the amount of DNA although the slope of the line is, as expected significantly greater for the linear DNA. The offsets of the two fitting lines represent the intensities of the background.
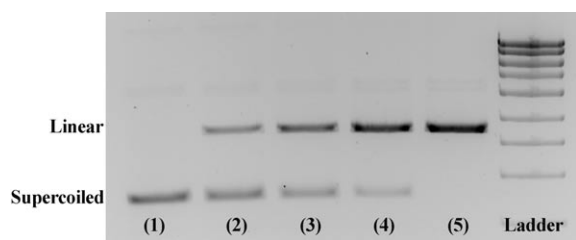
Figure 1. A photograph of the agarose gel used to separate various mixtures of supercoiled and linear pUC18 molecules.

If we assume that our sample of supercoiled pUC18 contains 100% of the supercoiled plectonemic form,[44] then we can find "the underfluorescent factor" for supercoiled pUC18 as the ratio between the slopes of the fitting lines in Figure 2:

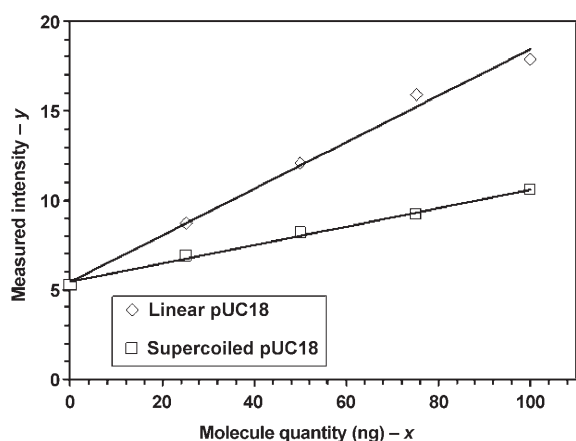$$R = \frac{0.1297}{0.0515} = 2.52 \qquad (1)$$

Figure 2. Correlation between fluorescence intensity and the amount of supercoiled (squares) and linear (diamonds) pUC18 plasmids measured from agarose gels after electrophoretic separation of the DNA. The solid lines are the least square fits to the data.

With the use of this factor, R, we can then compare the distributions of various topological forms of irradiated pUC18 as determined by gel electrophoresis and by AFM. To introduce SSBs and DSBs, samples of supercoiled pUC18 at a concentration of $1 \text{ ng } \mu L^{-1}$ were irradiated by γ-rays at doses of 1, 2, 5, and 10 Gy. Figure 3a shows a photograph of the agarose gel with untreated (control) and irradiated pUC18. Figure 3b and c shows the representative AFM images obtained in air, of untreated (control) pUC18 and pUC18 that were irradiated at a dose of 10 Gy. The AFM images were obtained after pUC18 had been deposited on the APS-mica surface from a buffer solution and dehydrated. From Figure 3b, we see that neither the binding to the mica surface nor the imaging action of the AFM tip significantly affected the DNA structure, which remained in the plectonemic supercoiled configuration. On the other hand, as seen from Figure 3c, the introduction of SSBs and DSBs
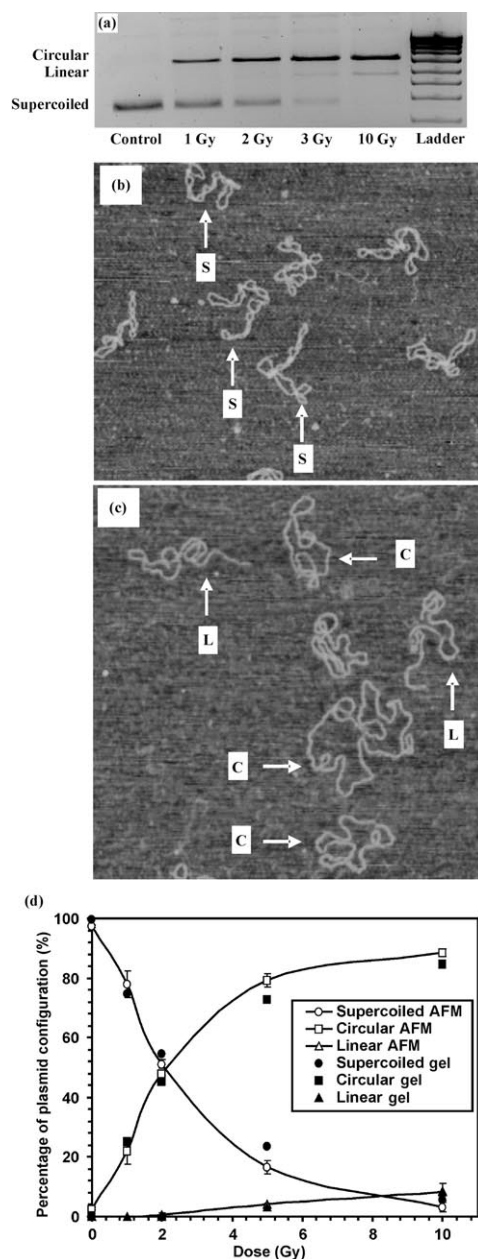

Figure 3. a) Photograph of untreated and irradiated pUC18 molecules ($1 \text{ ng } \mu L^{-1}$) at doses of 1–10 Gy following agarose gel electrophoresis, b) a representative AFM image of untreated pUC18, c) a representative AFM image of irradiated pUC18 at a dose of 10 Gy; the image size of (b) and (c) is 1 µm × 1 µm. d) Comparison between the results of DNA configuration distributions obtained by AFM imaging and agarose gel electrophoresis.

(irradiated sample) relaxed the molecules to their circular and linear forms, which can be easily identified in AFM images because of their distinct appearance (see the arrows in Figure 3b and c).[35] We determined the distributions of various topological fractions of irradiated pUC18 by counting the numbers of supercoiled (S), circular (C), and linear (L) molecules in AFM images. As can be seen from Figure 3d, the distribution of the three topological forms of

pUC18 obtained by AFM agrees well, within the metrology errors, with the corresponding distribution obtained by agarose gel electrophoresis, once the *R* factor was taken into account. Therefore, we conclude that our DNA damage-detection assay by AFM imaging is accurate and reliable, and can be confidently used for studying radiation damage to supercoiled plasmids.

2.2 Quantification of Single-Strand Breaks (SSBs)

In γ-radiation experiments, if we assume that all DNA molecules in the sample have an equal probability of developing radiation-induced strand breaks, and if the number of molecules is very large in comparison to the average number of strand breaks per molecules (*P*), the fraction of molecules having *N* single-strand breaks will follow the Poisson distribution,[45,46]

$$f(P, N) = \frac{P^N \exp(-P)}{N!} \tag{2}$$

The percentage of intact molecules, that is, supercoiled plasmid ($N = 0$), can then be found to be

$$f(P, 0) = \exp(-P) \tag{3}$$

Therefore, the average number of SSBs per molecule, *P*, can be obtained from

$$P = -\ln(f(P, 0)) \tag{4}$$

Thus, determining the fraction, *f*, of intact supercoiled DNA at a given radiation dose allows, according to Equation (4), the average number of SSBs per molecule to be found. Equation (4) can be used in conjunction with AFM imaging to determine SSBs per molecule. This can be done accurately, assuming that no more than one DSB per molecule is produced, because more DSBs would fragment the DNA and this, in turn, could possibly lead to errors in determining *f*.

2.3 The Effect of the Radiation Dose on the Number of SSBs

The dependence of DNA damage induced by γ-radiation on the radiation dose has been extensively studied, and the number of SSBs was found to be linearly proportional to the radiation dose.[6,40–43] Our results obtained using AFM imaging of supercoiled pUC18, irradiated at low and moderate doses (1–10 Gy) and low DNA concentrations (1 ng μL^{-1}) follow the same trend. Figure 4 shows that the number of SSBs per molecule (*P*), determined using Equation (4), is linearly correlated to the radiation dose (*D*). It is noted that the background number of SSBs, because of the presence of some relaxed plasmids in the "untreated" DNA sample (less than 4%), was deducted from the value obtained from irradiated plasmids, and the net SSBs per molecule are plotted in Figure 4.
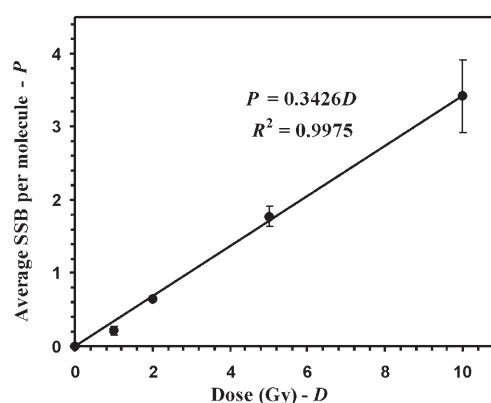

Figure 4. Correlation between average SSBs per molecule *P* and the radiation dose *D*. The DNA molecules used were supercoiled pUC18 at 1 ng μL^{-1}.

2.4 The Effect of the Plasmid Size on the Number of SSBs

In principle, if other conditions are kept the same, the larger the size of the plasmid, the higher the number of radiation-induced SSBs that are expected per molecule. Thus, the number of SSBs per molecule should be linearly proportional to the plasmid size, *S*. However, this hypothesis has not been carefully investigated and verified yet.[41] Here we irradiated three supercoiled plasmids with different sizes, i.e., pUC18 (2686 base pairs (bps)), phixi-174 (5386 bps) and pNEBR-R1 (10338 bps) and imaged them in an AFM to test this conjecture. In these experiments the plasmid concentration, *C*, was kept constant at 2 ng μL^{-1}, and the radiation dose, *D*, was 1 Gy. Figure 5a shows a representative AFM image of untreated pNEBR-R1 molecules, and Figure 5b shows an AFM image of irradiated pNEBR-R1 molecules, revealing intact supercoiled plasmids (S), relaxed circular plasmids (C) and linearized plasmids (L) (see the arrows in Figure 5a and b). The distributions of S, C, and L fractions of the three plasmids are shown in Figure 5c for the untreated DNA and in Figure 5d for the irradiated samples. From Figure 5d, it can be clearly seen that the percentage of intact molecules (S) in the irradiated samples decreases, while the percentage of relaxed molecules (C and L) increases with the increase in the DNA size. For instance, in irradiated pUC18, the fraction of relaxed molecules (C+ L) is 14.4%, and this number increases to 21.9% for phixi-174, and to 43.7% for pNEBR-R1 (after subtracting background damage). The average number of SSBs per molecule *P*, based on Equation (4), is shown to be linearly proportional to the DNA size *S* (Figure 5e), which verifies our initial conjecture.

2.5 DNA Damage-Dependence on Plasmid Concentration

In contrast to DNA size, the effect of DNA concentration on the amount of radiation damage is more complicated and follows a nonlinear trend.[41] We investigated this effect using pUC18, at various concentrations spanning three orders of magnitude, from 0.01 ng μL^{-1} to 10 ng μL^{-1}.
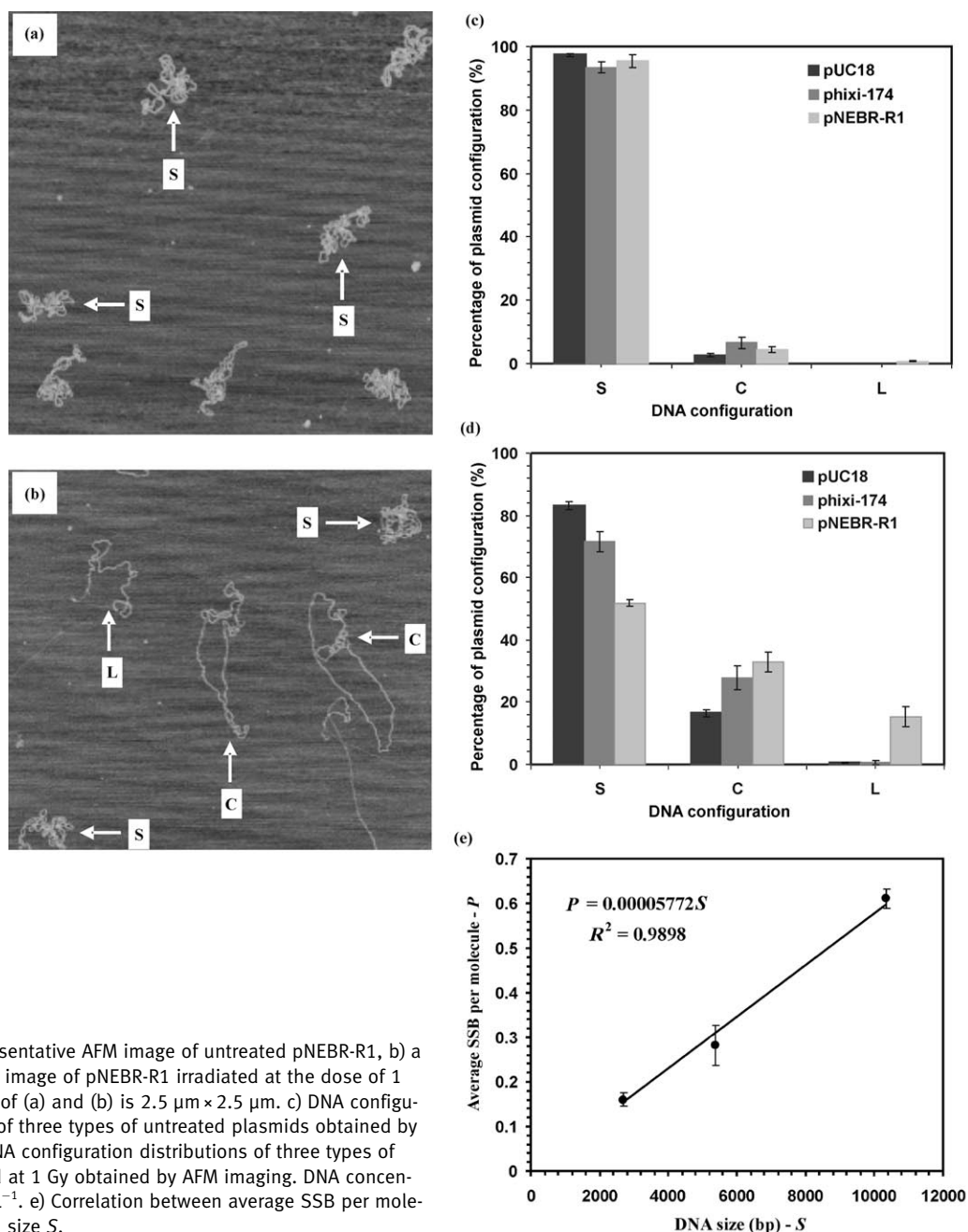
Figure 5. a) A representative AFM image of untreated pNEBR-R1, b) a representative AFM image of pNEBR-R1 irradiated at the dose of 1 Gy. The image size of (a) and (b) is 2.5 µm × 2.5 µm. c) DNA configuration distribution of three types of untreated plasmids obtained by AFM imaging. d) DNA configuration distributions of three types of plasmids irradiated at 1 Gy obtained by AFM imaging. DNA concentrations are 2 ng µL^{-1}. e) Correlation between average SSB per molecule P and plasmid size S.

It is worth noting that AFM imaging can be done directly on DNA originating from extremely dilute samples, which allowed us to explore a range of very low concentrations that have not been studied in the previous bulk irradiation measurements, because detecting DNA damage at a DNA concentration of 0.1 ng µl^{-1} or lower is generally beyond the capability of the traditional agarose gel electrophoresis technique. This observation suggests that AFM imaging, which excels on highly dilute samples, can uniquely supplement the traditional techniques for high-resolution measurements of ionizing radiation damage to DNA. The DNA was irradiated at the dose of 1 Gy, and Figure 6 shows the average number of SSBs per molecule at various DNA concentrations. The relationship between DNA concentration (C) and

the number of SSBs (P) can be satisfactorily fitted by a power function.

$$P = aC^b \tag{5}$$

in which a and b are fitting parameters. Figure 6 clearly indicates that the number of SSBs per molecule increases with the decrease in the DNA concentration. This observation is likely to reflect the fact that the number of free radicals generated per DNA molecule increases at lower DNA concentrations compared to greater DNA concentrations. On the other hand, the nonlinearity of this relationship suggests that at low DNA concentrations the mean free path of radicals increases as compared to higher DNA concentrations,
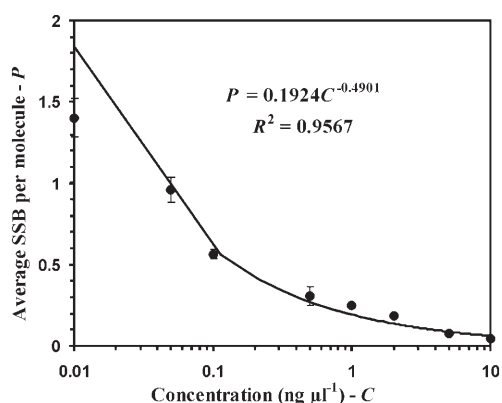
$P = 0.1924C^{-0.4901}$

$R^2 = 0.9567$

Figure 6. Correlation between average SSB per molecule P and DNA concentration C. The DNA molecules used were supercoiled pUC18 irradiated at 1 Gy.

and therefore the efficiency of the radical attack on DNA decreases at lower DNA concentrations.

3. Conclusions

In this paper, we used a novel implementation of the classical supercoiled plasmid relaxation assay on the AFM imaging platform for a sensitive detection of DNA damage caused by γ-radiation. Our results show that the AFM single-molecule assay is accurate and reliable, as verified by the well-established DNA damage-detection method, namely the agarose gel-electrophoresis technique. We examined the effect of radiation dose on the number of SSBs induced by γ-radiation and also quantitatively studied the dependence of DNA damage on DNA size and concentration, significantly extending the range of the latter parameter beyond the range accessible to bulk methods. At present, the AFM method is somewhat tedious and requires a trained user in both AFM imaging and image analysis; however, we believe that it will play an increasingly significant role supplementing traditional techniques for high-resolution measurements of ionizing-radiation damage to DNA.

4. Experimental Section

DNA: Supercoiled DNA plasmid pUC18 (2686 base pairs) was isolated from *E. coli* and purified using the Qia-Filter plasmid maxi kit (QIAGEN Inc.) following the manufacturer's instructions. Supercoiled DNA plasmid pNEBR-R1 (10338 base pairs) and supercoiled DNA plasmid phixi-174 (5386 base pairs) were purchased from New England Biolab, Inc. (Ipswich, MA). Linear pUC18 was produced by digesting pUC18 plasmids using EcoRI endonuclease purchased from New England Biolab, Inc. (Ipswich, MA).

Irradiation conditions: γ-irradiation was performed with the ^{137}Cs γ-rays (6.63 Gy min^{-1}) from the source in the Department of Radiation Biology at Duke University. 10 μL of

supercoiled DNA in 0.01 M phosphate buffer, 0.0027 M potassium chloride, and 0.137 M sodium chloride at concentrations of 0.01–10 ng μL^{-1} were exposed to gamma rays at room temperature for different times. Doses were calculated by multiplying gamma intensity by the exposure time.

Immobilization of DNA molecules for AFM imaging: 1-(3-Aminopropyl) silatrane-functionalized mica (APS-mica) was used for the binding of DNA molecules. APS-mica was prepared as described by Shlyakhtenko et al.[29] A drop of 2–5 μL of DNA solution (DNA concentration of 0.5–1 ng μL^{-1}) was deposited on APS-mica surface, at room temperature for 3 min. The sample was then rinsed and air-dried before imaging.

AFM imaging and image analysis: Images were taken by a Nanoscope IIIa MultiMode Scanning Probe Microscope (Veeco Instruments Inc., Santa Barbara, CA) using tapping mode with an E scanner. Rotated tapping-mode etched-silicone probes (RTESPs, Veeco) were used for imaging in air. The spring constant of AFM cantilevers was 20–80 Nm^{-1} and their resonance frequency was 275–316 kHz. All images were collected at a scan rate of 2.0–3.0 Hz, a scan line of 512×512 pixels, and scan sizes of 1 μm to 5 μm. In each experiment, 15–50 AFM images were captured and analyzed to determine the fractions of supercoiled (intact molecules), circular (containing SSBs), and linear (generated by DSBs) molecules. The results are expressed as the mean ± standard deviation for each fraction. As before,[35] we assumed that pUC18 molecules with a number of supercoiled nodes greater than five are intact, while the number of nodes equal to or less than five was indicative of structural alterations within supercoiled DNA. By this criterion, untreated pUC18 DNA samples contained $\geq 96 \pm 1\%$ of intact supercoiled DNA. This high percentage of intact DNA is important in order to reliably quantify DNA damage caused by gamma radiation. To verify further the accuracy of our assay that is based on a visual inspection of AFM images we also determined the difference between the results obtained by different persons, on the same data set, and found it was less than 5%.[35]

Gel electrophoresis: DNA was separated on 1% agarose gel in the presence of 10 μg mL^{-1} ethidium bromide in TBE Buffer (89 mM Tris borate, 2 mM ethylenediaminetetraacetate (EDTA), pH 8.3). Gel images were taken using 8-bit CCD camera (Gel Doc EQ system, Bio-Rad Laboratories, Inc.) and they were analyzed using the Quantity One software (Bio-Rad Laboratories, Inc.).

[1] F. A. Mettler, G. L. Voelz, *N. Engl. J. Med.* **2002**, *346*, 1554–1561.

[2] J. K. Waselenko, T. J. MacVittie, W. F. Blakely, N. Pesik, A. L. Wiley, W. E. Dickerson, H. Tsu, D. L. Confer, C. N. Coleman, T. Seed, P. Lowry, J. O. Armitage, N. Dainiak, *Ann. Intern. Med.* **2004**, *140*, 1037–1051.

[3] H. K. Dressman, G. G. Muramoto, N. J. Chao, S. Meadows, D. Marshall, G. S. Ginsburg, J. R. Nevins, J. P. Chute, *PLoS Med.* **2007**, *4*, 690–701.

[4] E. C. Friedberg, G. C. Walker, W. Siede, *DNA Repair and Mutagenesis*, ASM Press, Washington, D.C. **1995**, pp. 19–24.

[5] J. F. Ward, *Prog. Nucleic Acids. Mol. Biol.* **1988**, *35*, 95–125.

[6] B. M. Sutherland, P. V. Bennett, O. Sidorkina, J. Laval, *Proc. Natl. Acad. Sci. U.S.A.* **2000**, *97*, 103–108.

[7] K. Psonka, S. Brons, M. Heiss, E. Gudowska-Nowak, G. Taucher-Scholz, *J. Phys.: Condens. Matter* **2005**, *17*, S1443–S1446.

[8] Y. L. Lyubchenko, L. S. Shlyakhtenko, *Proc. Natl. Acad. Sci. U.S.A.* **1997**, *94*, 496–501.

[9] M. Murakami, H. Hirokawa, I. Hayata, *J. Biochem. Biophys. Methods* **2000**, *44*, 31–40.

[10] K. Rothkamm, M. Lobrich, *Proc. Natl. Acad. Sci. U.S.A.* **2003**, *100*, 5057–5062.

[11] D. Pang, J. E. Rodgers, B. L. Berman, S. Chasovskikh, A. Dritschilo, *Radiat. Res.* **2005**, *164*, 755–765.

[12] M. A. Siddiqi, E. Bothe, *Radiat. Res.* **1987**, *112*, 449–463.

[13] W. M. Chen, E. R. Blazek, I. Rosenberg, *Med. Phys.* **1995**, *22*, 1369–1375.

[14] E. C. Friedberg, G. C. Walker, W. Siede, *DNA Repair and Mutagenesis*, American Society for Microbiology, Washington, DC, **1995**, pp. 23–24.

[15] S. E. Freeman, A. D. Blackett, D. C. Monteleone, R. B. Setlow, B. M. Sutherland, J. C. Sutherland, *Anal. Biochem.* **1986**, *158*, 119–129.

[16] Y. F. Maa, S. C. Lin, C. Horvath, U. C. Yang, D. M. Crothers, *J. Chromatogr.* **1990**, *508*, 61–73.

[17] S. X. Zheng, G. L. Newton, J. F. Ward, R. C. Fahey, *Radiat. Res.* **1992**, *130*, 183–193.

[18] J. H. Vantouw, J. B. Verberne, J. Retel, H. Loman, *Int. J. Radiat. Biol.* **1985**, *48*, 567–578.

[19] B. M. Sutherland, P. V. Bennett, K. Conlon, G. A. Epling, J. C. Sutherland, *Anal. Biochem.* **1992**, *201*, 80–86.

[20] M. Rosemann, B. Kanon, A. W. T. Konings, H. H. Kampinga, *Int. J. Radiat. Biol.* **1993**, *64*, 245–249.

[21] J. K. Sandhu, H. C. Birnboim, *Radiat. Res.* **1993**, *135*, 338–342.

[22] W. C. Dewey, L. L. Thompson, M. L. Trinh, D. L. Latz, J. F. Ward, *Radiat. Res.* **1994**, *140*, 37–47.

[23] S. C. Prasad, J. Boyle, A. Dritschilo, *Radiat. Res.* **1989**, *117*, 538–546.

[24] G. Binnig, C. F. Quate, C. Gerber, *Phys. Rev. Lett.* **1986**, *56*, 930–933.

[25] H. G. Hansma, *Annu. Rev. Phys. Chem.* **2001**, *52*, 71–92.

[26] Y. Lyubchenko, L. Shlyakhtenko, R. Harrington, P. Oden, S. Lindsay, *Proc. Natl. Acad. Sci. U.S.A.* **1993**, *90*, 2137–2140.

[27] Y. L. Lyubchenko, A. A. Gall, L. S. Shlyakhtenko, S. M. Lindsay, *Biophys. J.* **1996**, *70*, WAMG6–WAMG6.

[28] M. Bussiek, N. Mucke, J. Langowski, *Nucleic Acids Res.* **2003**, *31*, e137

[29] L. S. Shlyakhtenko, A. A. Gall, A. Filonov, Z. Cerovac, A. Lushnikov, Y. L. Lyubchenko, *Ultramicroscopy* **2003**, *97*, 279–287.

[30] L. S. Shlyakhtenko, L. Miloseska, V. N. Potaman, R. R. Sinden, Y. L. Lyubchenko, *Ultramicroscopy* **2003**, *97*, 263–270.

[31] S. Boichot, M. Fromm, S. Cunniffe, P. O'Neill, J. C. Labrune, A. Chambaudet, E. Delain, E. Le Cam, *Radiat. Prot. Dosim.* **2002**, *99*, 143–145.

[32] D. Pang, B. L. Berman, S. Chasovskikh, J. E. Rodgers, A. Dritschilo, *Radiat. Res.* **1998**, *150*, 612–618.

[33] D. Pang, B. Vidic, J. Rodgers, B. Berman, A. Dritschilo, *Radiat. Oncol. Invest.* **1997**, *5*, 163–169.

[34] D. Pang, B. L. Berman, S. Chasovskikh, J. E. Rodgers, A. Dritschilo, *Radiat. Res.* **1999**, *152*, 106–106.

[35] Y. Jiang, C.-H. Ke, P. A. Mieczkowski, P. E. Marszalek, *Biophys. J.* **2007**, *93*, 1758–1767.

[36] Y. Yoshikawa, K. Hizume, Y. Oda, K. Takeyasu, S. Araki, K. Yoshikawa, *Biophys. J.* **2006**, *90*, 993–999.

[37] M. Folkard, K. M. Prise, C. J. Turner, B. D. Michael, *Radiat. Prot. Dosim.* **2002**, *99*, 147–149.

[38] M. Folkard, K. M. Prise, B. Vojnovic, B. Brocklehurst, B. D. Michael, *Int. J. Radiat. Biol.* **2000**, *76*, 763–771.

[39] J. H. Parish, *Principles and Practice of Experiments with Nucleic Acids* Wiley, New York, **1972**.

[40] K. Hempel, E. Mildenberger, *Int. J. Radiat. Biol.* **1987**, *52*, 125–138.

[41] C. Giustranti, C. Perez, S. Rousset, E. Balanzat, E. Sage, *J. Chim. Phys. Phys.-Chim. Biol.* **1999**, *96*, 132–137.

[42] A. Ozols, K. M. Prise, B. D. Michael, *Int. J. Radiat. Biol.* **1999**, *75*, 83–90.

[43] B. M. Sutherland, P. V. Bennett, N. Cintron-Torres, M. Hada, J. Trunk, D. Monteleone, J. C. Sutherland, J. Laval, M. Stanislaus, A. Gewirtz, *J. Radiat. Res.* **2002**, *43*, S149–S152.

[44] In reality, direct AFM imaging of our pUC18 samples indicates that <4% of the plasmids are in the relaxed circular form, which is consistent with the observed small amount of damage introduced when purifying pUC18 using the QiaFilter plasmid maxi kit (see the section "AFM imaging and image analysis" in the Experimental Section and Reference [35]).

[45] P. N. Lobachevsky, T. C. Karagiannis, R. F. Martin, *Radiat. Res.* **2004**, *162*, 84–95.

[46] R. K. Sachs, A. L. Ponomarev, P. Hahnfeldt, L. R. Hlatky, *Math. Biosci.* **1999**, *159*, 165–187.